Extensional deformation, cohesive failure, and boundary conditions during sharkskin melt fracture

K. B. Migler,[a] Y. Son, F. Qiao, and K. Flynn

Polymers Division, National Institute of Standards and Technology, 100 Bureau Drive, Gaithersburg, Maryland 20899-8544

(Received 5 June 2001; final revision received 13 November 2001)

Synopsis

We measure the flow kinetics of a polyethylene extruded through the exit of a sapphire capillary tube in order to understand the nature of sharkskin, a surface roughness in the extruded material. Optical velocimetry shows that sharkskin can occur under a variety of polymer/wall boundary conditions; stick, slip, or oscillating stick/slip, demonstrating that the flow boundary condition is not the direct cause of sharkskin. Downstream of the exit, high-speed video microscopy reveals two distinct material failures during each sharkskin cycle, the first is cohesive and splits the material into two regions, the second one occurs at the polymer–wall interface. Upon modification of the surface with a polymer processing additive (PPA), we confirm strong slip at the wall and a suppression of sharkskin, but find that sharkskin does return at sufficiently high flow rates. The extensional strain rate at the onset of sharkskin is significantly higher in the case with PPA than that without. We then empirically define a ''reconfiguration rate'' and find it is comparable at the onset of sharkskin for the two surface conditions. We use data in the literature to show that the reconfiguration rate also predicts the relationship observed between the onset of sharkskin and the capillary radius. [DOI: 10.1122/1.1445186]

INTRODUCTION

Over the past 50 years, there has been a sustained interest in the understanding and control of instabilities that occur upon pressure driven extrusion of molten polymers. These instabilities limit the manufacturing rate and the materials selection in continuous forming operations, such as sheet extrusion. Processors are forced to sacrifice final mechanical properties to achieve greater processability. From the scientific point of view, understanding of these instabilities is challenging; despite much progress, fundamental issues remain unresolved. An understanding of the cause of sharkskin would enable a more rational design of materials in order to eliminate it.

In the case of extrusion through a capillary die, at sufficiently low extrusion rates, the polymer is smooth as it exits the die. At progressively higher extrusion rates, a series of flow instabilities occurs. The first instability that *may* occur is known as *sharkskin* or sharkskin melt fracture and is characterized by surface roughness. At higher extrusion rates, one observes an oscillating *stick–slip* transition, followed at higher rates by *gross melt fracture* in which the polymer is extruded in an extremely irregular fashion. The occurrence of the instabilities is dependent on many factors including polymer chemistry,

[a]Author to whom all correspondence should be addressed; Electronic mail: kalman.migler@nist.gov

architecture, molecular weight and distribution, and polymer/wall surface interactions. A review and history of this subject has recently been written [Denn (2001)].

In this work we focus on the sharkskin instability. The driving force behind the attempts to understand sharkskin is that linear chain polyethylenes of narrow molecular weight distribution are particularly susceptible to this instability. Because this instability occurs at relatively low extrusion rates, it is troublesome. The subject has received renewed attention because the newer metallocene based polyethylenes offer advantages in mechanical properties but often suffer from this extrusion instability due to their inherently narrow molecular weight distribution. There have been numerous suggestions for the mechanism of sharkskin and for elucidation of the conditions that produce it. We review several interrelated issues that are central to understanding sharkskin.

The first issue is the location of the initiation of sharkskin. There is strong evidence that the exit of the capillary tube serves as the initiation point, as was first suggested 40 years ago by [Howells and Benbow (1962)]. Recent evidence comes from stress birefringence experiments which show a sharp peak in the stress distribution at the exit due to velocity rearrangements that occur in the material as it makes the transition from inside the capillary (pressure-driven flow) to outside it (plug flow). This observation has been made in polybutadiene [Piau *et al.* (1995)], in PDMS [El Kissi *et al.* (1997)], and in polyethylene [Mackley *et al.* (1998)]. During sharkskin, the stress birefringence just upstream of the exit has been shown to oscillate [Barone and Wang (1999); El Kissi *et al.* (1997)]. Furthermore, numerical models also show the existence of large stress and elongational fields in the exit region [Rutgers and Mackley (2000); Tremblay (1991); Venet and Vergnes (2000)]. The sharp exit corner produces a singularity in the mathematical models. It is well known that incorporation of a low energy surface to the very exit of the tube can eliminate sharkskin [Inn *et al.* (1998); Moynihan *et al.* (1990)]. The flow in the tube itself during sharkskin conditions has been shown to be smooth [Inn *et al.* (2000); Migler *et al.* (2001)].

A major focus of recent efforts is to understand the connection between the flow boundary conditions and sharkskin. Upstream of the capillary exit, several reports indicate that, during sharkskin, the polymer slips at the wall [Kalika and Denn (1987); Ramamurthy (1986)]. Tzoganakis *et al.* (1993) concluded via capillary rheology that the onset of slip occurs at a lower wall shear stress than the onset of sharkskin. However, others have shown that it sticks at the wall [El Kissi and Piau (1994); Ghanta *et al.* (1999); Migler *et al.* (2001)].

Several authors have hypothesized that the boundary condition may be different at the capillary exit than in the interior (die land). For example, it has been proposed that the slippage can be greater near the exit [Hatzikiriakoks and Dealy (1992)]. Others have suggested that the polymer sticks in the capillary die but that the boundary condition at the exit oscillates in time between slip and stick. (This local instability is distinct from the stick–slip transition discussed in the second paragraph in which the slippage occurs throughout the die) [Wang *et al.* (1996).] Another idea is that the contact line between the polymer, the wall, and the atmosphere oscillates at the die exit [Dhori *et al.* (1997)].

By changing the boundary condition to favor slippage, it has been shown that sharkskin is eliminated [El Kissi *et al.* (1994); Hatzikiriakos *et al.* (1995); Moynihan *et al.* (1990); Piau *et al.* (1995)]. Fluorocopolymer additives have been used industrially since the 1960s to reduce/eliminate sharkskin and have been intensely studied [Amos *et al.* (2001)]. Recently Migler *et al.* (2001) confirmed through direct observation that they migrate to the internal capillary wall and induce slippage between themselves and the main polymer (a polyethylene). They found that the fluoropolymer induces a slip boundary condition, which in turn causes a dramatic reduction in the total extensional defor-

mation in the polyethylene at the surface as it exits the tube. It was concluded that it is this reduction in extensional deformation (rather than the reduction in shear rate or the occurrence of slippage) that causes fluoropolymer additives to suppress sharkskin. It has also been shown that replacing a steel capillary with other materials (brass, aluminum, copper, glass, etc.) can affect sharkskin [Ghanta *et al.* (1999); Person and Denn (1997); Ramamurthy (1986)]. Interestingly, when Wise *et al.* (2000) utilized a Teflon capillary (which induces slippage), they reported that sharkskin is not eliminated, rather its onset is shifted to significantly higher shear stress (and apparent wall shear rate).

The next question is about the cause of the rough surface. This is intimately related to the boundary conditions. For the oscillating localized stick–slip hypothesis, it is the boundary condition at the wall itself that causes the surface undulations seen in the extrudate. Barone *et al.* (1998) argued that the ridges are created by the increased stress (hence die swell) that occurs when the material sticks whereas the valleys are created when the material slips (reduced die swell), although Barone *et al.* (1999) seemed to suggest a different picture. An alternative hypothesis is that flow discontinuity at the exit occurs due to high stress levels; this was made popular by simple arguments advanced by Cogswell (1977). This discontinuity goes by several names, such as tearing, rupture, and cracking. If one considers a stick boundary condition, the polymer very near the surface undergoes great stretching as its velocity rapidly increases from near zero inside the tube to a finite value outside the tube. In this model, the extensional stress outside the die is so great that the material tears. Since the extensional stress is greatest at the surface, the tear starts there and propagates into the material. The tear creates a flow discontinuity and splits the material into two distinct layers; the layer near the wall becomes the ridges and that in the core becomes the valleys. In a related model, Tremblay suggested that the material undergoes cavitation due to the extensional stresses rather than tearing. Both models are similar in that there is a cohesive flow discontinuity caused by the extensional nature of the flow at the exit.

There is reasonable evidence to support the Cogswell picture. Sharkskin visualization experiments in PDMS [El Kissi *et al.* (1997); Howells and Benbow (1962)] and in polybutadiene [Inn *et al.* (1998)] have been interpreted in terms of a two-layer model or of a tearing/rupture mechanism. Rutgers and Mackley (2000) have shown a correlation between the stress at breakage of a stretched fiber and the numerically calculated extensional stress on the material near the wall at the capillary's exit. A simple experiment to test for flow discontinuity is to color the polyethylene near the internal surface of the die and leave colorless the material in the core. It was found that the ridges were colored whereas the valleys were clear, an indication of a flow discontinuity caused by tearing [Barone *et al.* (1999), Cogswell (1977)]. A further test of this model is to understand why the fluoropolymer additives reduce sharkskin. As discussed above, Migler *et al.* (2001) showed that the additives eliminate sharkskin by dramatically reducing the extensional stretching at the exit, that is, in accord with the Cogswell model.

The physical parameter that coincides with the onset of sharkskin has not been identified. Cogswell proposed that the extensional strain rate is the controlling parameter but, in his ''silly putty'' experiments, as the radius increases by a factor of 4, the extensional strain rate decreases by a factor of 0.6. While the Cogswell model argued that when extensional stress at the air–polymer interface at the exit exceeds a critical parameter rupture should occur, such a localized quantitative measure has not yet been made. Recoverable strain has also been suggested as the critical parameter [Pomar *et al.* (1994)]. However, this parameter does not agree with the observation of the inverse dependence of the shear rate at the onset of sharkskin with the radius of the die.

We close the review by adding that recent efforts to suppress sharkskin involve modification of the exit die geometry [Kulikov and Hornung (2001)], novel processing additives [Hong *et al.* (1999); Rosenbaum *et al.* (2000)], and modification of the die material [Ghanta *et al.* (1999)].

It is the aim of this work to try to distinguish between the various possibilities described above. Many of these ideas can be tested through a combination of microvelocimetry, optical imaging, and surface modification through fluoropolymer additives. We further seek to conduct the experiments under conditions of maximum industrial relevance by use of a metallocene polyethylene processed by twin-screw extrusion.

In this article, we conduct microvelocimetry measurements in the vicinity of the capillary exit under conditions that produce sharkskin instability. Measurements conducted upstream of the exit serve to probe the flow boundary condition at the polymer/wall interface. In particular, we check whether sharkskin is associated with a slip boundary condition, a stick boundary condition, or an oscillating stick/slip. We conduct these experiments on two sets of boundary conditions, first, on one with strong polymer wall interaction, then when the interaction is weakened by the presence of a fluoropolymer at the wall.

Next, we conduct visualization studies of the sharkskin kinetics. These measurements serve two purposes; first, we wish to understand what gives rise to the rough surface. Second, we ask whether the kinetics in polyethylene sharkskin is similar to that in previously studied model materials (polybutadiene and polydimethylsiloxane).

Finally, we conduct measurements of the extensional strain rate at the onset of sharkskin for the weak and strong boundary conditions. Here, we seek a parameter that coincides with the onset of sharkskin. One clue from the work of Migler *et al.* (2001) is that the fluoropolymer slip layer greatly reduces the extensional stretching at the die lip. Further, there is a wide processing window in which, for a constant *true* wall shear rate, the strong boundary condition produces sharkskin and the weak (fluoropolymer) boundary condition produces a smooth extrudate. It was suggested that an interesting parameter to consider is the rate of change of the extensional flow for the two boundary conditions. In the current work we increase the flow rate so that sharkskin is produced under the weak boundary conditions and propose an empirical parameter for the onset of sharkskin.

EXPERIMENT

In previous work, Migler *et al.* (2001) utilized a sapphire capillary die situated at the exit of a twin-screw extruder. A microscope with stroboscopic illumination was constructed at the capillary die exit in order to image the flow. Particle tracking velocimetry was utilized to measure the velocity of a metallocene polyethylene polymer as a function of the radius inside the capillary for a series of extrusion rates. It was found that this polymer sticks at the wall, and that sharkskin is observed at low extrusion rates. Following addition of a fluoropolymer process additive at low concentration to the linear low-density polyethylene (LLDPE), it was observed through direct real-time microscopic imaging that the fluoropolymer coats the internal surface in a streak pattern. The LLDPE was observed to slip against the fluoropolymer via polymer–polymer slippage, concomitant with the elimination of sharkskin. Those experiments were conducted at 210 °C 3 mm upstream of the die exit.

In the current work, the apparatus has been modified in several ways. First, we attach a high-speed video camera (1000 frames/s) to our microscope which allows observation of the sharkskin dynamics in polyethylene with high temporal and spatial resolution. Second, the objective lens of the microscope is now mounted on a three-dimensional

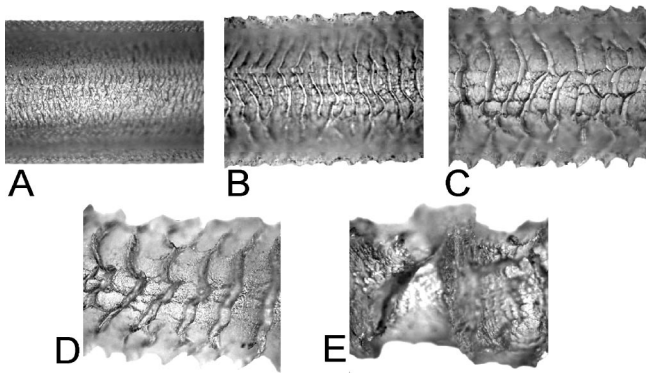

FIG. 1. Cold postextrusion micrographs as a function of the flow rate. The processing conditions were $T = 177\,^{\circ}\mathrm{C}$ and no PPA. Each image is actually a composite of two micrographs in which the side and top are focused. The relative errors in throughputs are 0.05 Q = (A) 1.0, (B) 2.2, (C) 3.8, (D) 6.3, and (E) 11 g/min. The width of each image corresponds to 3 mm.

translation stage, so that measurements can be easily made as a function of the distance along the capillary flow axis (both upstream and downstream of the exit.) In this experiment the slowest moving particles are those closest to the wall; by focusing the objective lens on these particles, we thus determine the position of the wall. By translating the objective lens relative to the wall position we make measurements at other radial positions. The length of the tube is $L = 33$ mm and the radius is $R = 0.80$ mm.

The experiments were carried out using the same polymer and fluoropolymer as Migler *et al.* (2001), a well-stabilized commercially available polyolefin *m*LLDPE (AFFINITY™ EG 8100 Polyolefin Plastomer) (see the Acknowledgment). It is characterized by a melt index of 1.0 and a density of 0.870 g/cm^3. This material was selected for its clarity, its overall low level of additives, and the absence of PPA in its formulation. In order to work at conditions where the sharkskin instability is relatively strong, we use the low temperature of 177 °C (and of 157 °C in one case), which is well below the recommended processing temperature of this material. The processing additive used in this study was a commercially available copolymer of hexafluoropropylene and vinylidene fluoride (Dynamar™ PPA-FX-9613). A master batch was prepared of a mass fraction of 3% PPA added to a commercially available 2.0 MI LLDPE through tumble blending (Ampacet). The master batch was tumble blended with the *m*LLDPE to achieve a mass fraction of PPA of 0.1%. Before the test, the equipment was purged using a commercially available purge compound (HM-10, Heritage Plastics) comprising a mass fraction of 70% $CaCO_3$ in a 10 MI LDPE.

SHARKSKIN WITH STRONG POLYMER/WALL INTERACTIONS

We seek to establish the nature of the polymer flow during sharkskin instability both upstream and downstream of the exit. Figure 1 shows a series of micrographs of cold-quenched extrudates. These micrographs are typical of what one finds in the literature: the severity of sharkskin increases with an increase in the mass flow rate. At the highest flow rate, (Fig. 1E), a second instability called gross melt fracture is observed.

First, we examine the connection between slippage and sharkskin. In the work of Migler *et al.* (2001) it was shown that sharkskin can occur in the absence of any slippage in the die land. Those measurements were taken 3 mm upstream of the exit. In the current work, those measurements are conducted much nearer the exit. We show in Fig. 2 the

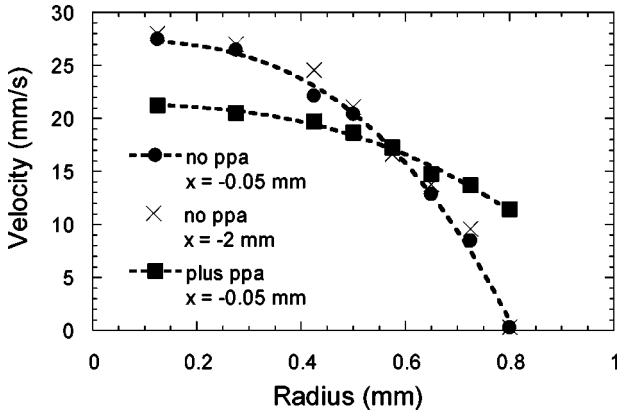

FIG. 2. Flow velocimetry as a function of the radial position of the polyethylene *inside* the capillary die for a flow rate $Q = 2.2$ g/min [the same as in Fig. 1(B)]. The measurements were conducted at $x = -0.05$ and -2 mm upstream of the exit. Also shown in the case with PPA.

velocity profile as a function of radius of the LLDPE in the absence of any polymer process additives. These experiments were taken at 177 °C, at a mass throughput of $Q = 2.2$ g/min; thus the extrudate corresponds to that seen in Fig. 1(B). The error in the radial direction is due to the finite depth of field, D, and the relative standard deviation of the velocities is 5%, and apply to all the velocity profile curves in this article. The relative standard deviation of the mass throughput is 7%, caused by fluctuations of the extruder. Under these conditions, the surface roughness that characterizes sharkskin is readily apparent. In Fig. 2, the measurements are taken at two axial positions: $x = -2$ and -0.05 mm. We take $x = 0$ to be the exit of the tube and the direction of flow is in the $+x$ direction so that $x = -0.05$ mm corresponds to a point 50 μm upstream of the exit. It is seen that the velocity profiles between these two measurements are very similar, indicating that the flow profile does not change appreciably even though the material is very near the exit. Further, it can be seen that the velocity of the slowest moving particles nearest the wall is near zero (on a linear scale).

We now consider the possibility of oscillating slip–stick behavior at the exit. We track single particles that are near the capillary wall over time roughly equal to one period of sharkskin. The particles that are within a few micrometers of the wall are moving so slowly that their motion is not clearly resolvable over this time interval of $T_{ss} \approx 30$ ms. In Fig. 3, we track the motion of several particles under the same flow conditions as those Figs. 1(B) and 2 (no PPA). By measuring their velocity, we can use the curve fit from Fig. 2 to deduce their distance from the wall, which is indicated in Fig. 3. We see in all cases that the position increases linearly over time rather than by stick–slip motion. For the slowest moving particle (5 μm from the wall), its velocity was deduced by observation of its motion over a longer period of time, so there was sufficient spatial resolution to measure the change in distance. These results agree with the observations in polybutadiene at the exit region [Inn *et al.* (2000)]. Furthermore, given the severity of the sharkskin distortion at the micron length scale, it is difficult to imagine that stick/slip could occur in the last 20 μm but not be felt at $x = -0.05$ mm. The condition of flow continuity would demand that effects of stick/slip be felt a modest 30 μm upstream of it. Thus we conclude that sharkskin can occur even though there is no stick–slip instability in the exit region. (Later we show different behavior at a lower temperature.)

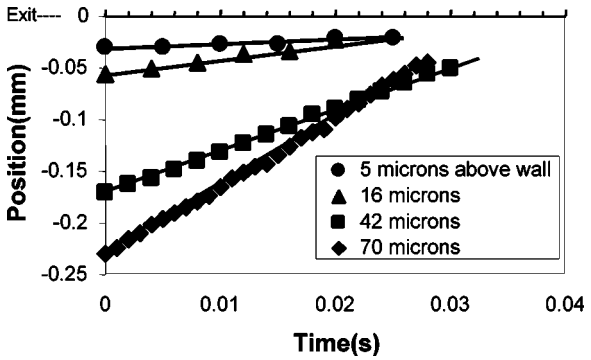

FIG. 3. Position-time curves for single particles as a function of the axial position in the vicinity of the die's exit. The different curves correspond to particles of different radial position. The time lapse from the first measurement at $t = 0$ s to the last one at $t \approx 25$ ms corresponds to approximately one cycle of sharkskin. The height of the particle from the wall is determined by flow curve fitting. Conditions: $Q = 2.2$ g/min and no PPA [the same as in Fig. 1(B)].

Now we reexamine the question of slippage at the wall near the exit. Measurements of the velocimetry as a function of the radial position for a series of mass flow rates were conducted 200 μm upstream of the exit. The velocimetry curves are shown in Fig. 4, along with fits to the power law model. Given the precision of the data, it is not appropriate to examine more sophisticated models. We again see that the velocities become small at the wall. The apparent wall shear rates for this plot are 55, 122, 210, and 348 s^{-1}. A measure of the degree of slippage is given by the extrapolation length, $b = v_s/\dot{\gamma}_w$ where in this case v_s is the velocity of the slowest moving particles that are observed and $\dot{\gamma}_w$ is the wall shear rate. We obtain $\dot{\gamma}_w$ through a fit of the data to a power law flow model (solid lines in Fig. 4). We obtain $b = 1.5$ μm for the slowest throughput, a value that is at the resolution limit of the apparatus. For the highest flow rate, we obtain $b = 17$ μm which indicates mild slippage. If there is any slippage, one considers the ratio b/R, where R is the radius of the capillary tube. This quantity measures the importance of the slippage to the rheology. For the highest flow rate, $b/R = 0.02$ which indicates that the slip is only marginally relevant to it. See the work of Migler *et al.*

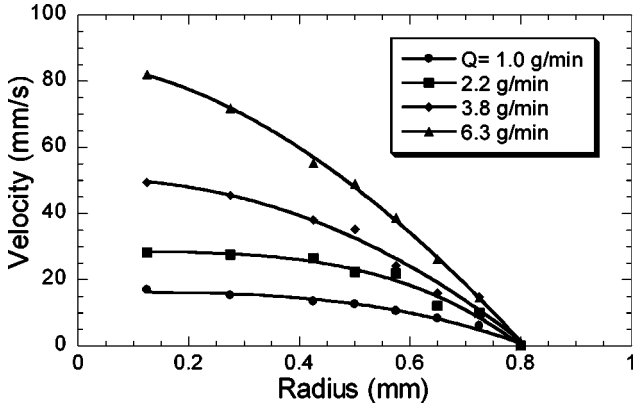

FIG. 4. Flow velocimetry as a function of the radial position of the polyethylene *inside* the capillary die for a series of flow rates. Measurements were taken at $x = -0.2$ mm (no PPA).

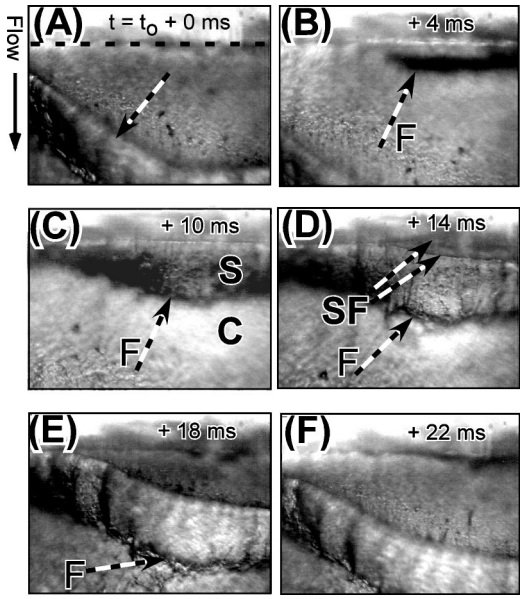

FIG. 5. High-speed video microscopy images of the evolution of the sharkskin structure. This sequence corresponds to one cycle of the sharkskin structure. The flow is downward; the exit of the die is shown by the dotted line at the top of the first time frame. The height of the micrograph corresponds to 340 μm. Conditions: $Q = 3.8$ g/min and no PPA. [The same as in Fig. 1(C)]. An on-line video of Fig. 5 is available: EPAPS Document No. E-JOR-HD2-46-003202.

(2001) for a discussion of the accuracy of the measurement of b when $b/R \ll 1$. We conclude that sharkskin can occur under conditions of *both* no slip and weak slip. Later we show that sharkskin can even occur during strong slip.

The images in Fig. 5 show one cycle of sharkskin instability. An on-line video of Fig. 5 is available via EPAPS Document EPA46 No. E-JOR HD2-46-003202. The flow conditions here are the same as those in Fig. 1(C). As will be shown below, an interesting feature is that there are two failures, a cohesive failure and a surface failure. In Fig. 5(A) ($t = t_0$), the extrudate is shown exiting the capillary tube. The horizontal dashed line shows the location of the edge of the capillary tube, which is the same for all six video micrographs. The flow direction is from top to bottom as shown by the arrow to the left of Fig. 5(A). At the bottom of Fig. 5(A), the surface disturbance from the previous cycle of sharkskin is visible (see the dashed arrow). By measuring the velocity of the extrudate in the first 50 μm downstream of the lip of the exit at this point in the cycle, we find the extensional strain rate to be $\dot{\varepsilon} \approx 500\,\mathrm{s}^{-1}$. In Fig. 5(B), ($t = t_0 + 4$ ms) we see the failure labeled ''F'' occurring at the air–polymer–tube contact line. In subsequent images this ''fracture line'' (always labeled as F) moves downstream until in Fig. 5(F) it is below the field of view. In Fig. 5(C), we see that the fracture surface divides the material into two regions, a surface layer (labeled S) and a core region (labeled C). The surface layer bulges upwards. In Fig. 5(C), the velocity of the surface region in the immediate vicinity of the exit lip (20 μm) is near zero, thus we say that the surface region sticks to the tube at this point in the cycle. The material in the growing surface region is composed of polymer that had been adjacent to the capillary wall while inside the capillary tube and the material in the core region is composed of polymer that had been at a smaller radius. In Figs. 5(B) and 5(C) fracture line F is a point of material discontinuity—the velocity of

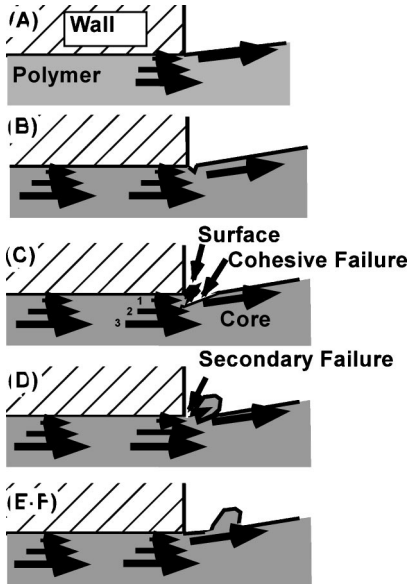

FIG. 6. Sketch of the kinetics of the sharkskin instability, side view. The labels on the images coincide with those in Fig. 5.

the core region is significantly greater than that of the surface region. (A plot of the velocimetry at the fracture line is presented later in Fig. 9.)

The splitting of the polymer into core and surface layers and the discontinuity in velocity at that interface (coupled with the coloration experiments) are the primary reasons for calling this a cohesive failure. The surface layer grows in size from Fig. 5(B) to Fig. 5(C) as time progresses. Next, in Fig. 5(D) ($t = t_0 + 14$ ms), the surface layer detaches from the capillary tube (the upper point labeled ''SF'' corresponds to the lip of the tube and the lower point labeled SF corresponds to the material that has detached from the tube.

Once the material has detached from the tube, fracture line F in Fig. 5(D) is no longer a point of material discontinuity—the velocity of the core and surface at this line become identical. Figures 5(E) and 5(F) show this failure line flowing. Meanwhile, back at the tubes lip area, once the failure line is not active, the extensional stress once again starts to build up. Figure 5(F) is essentially the same point in the sharkskin cycle as Fig. 5(A).

With regard to initiation of the fracture line in Fig. 5(B), it is not correct to say that the fracture occurs spontaneously from a locally ''smooth'' material. The arrow in Fig. 5(B) shows the initiation of fracture. To the right of this point, the fracture line is visible, while to the left, fracture has not yet occurred. In Fig. 5(C) the initiation point is at the leftmost part of the image. The initiation point propagates circumferentially around the capillary tube; it could equally well propagate from left to right. It seems reasonable to assume that the stress to continue the propagation of an existing fracture line is less than the stress required to propagate a new fracture line. When the initiation point travels undisturbed around the circumference for several cycles of sharkskin, the sharkskin ridges spiral around the extrudate.

A side-view cartoon of our interpretation of the kinetics is shown in Fig. 6. In Fig. 6(A), the polymer's jump in velocity from the polymer–tube interface to the polymer–air interface is depicted. The extensional stress at the air–polymer–sapphire contact line builds up over time until the material fractures, Fig. 6(B). The fracture is located at the

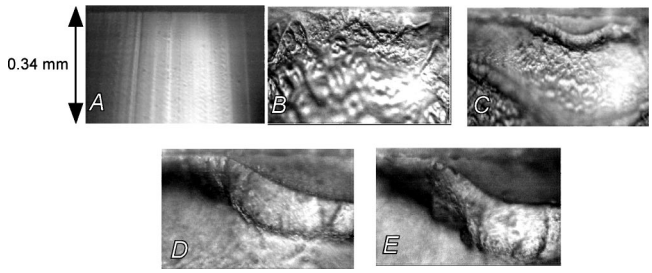

FIG. 7. High-speed video microscopy images as a function of the flow rate. No PPA. Q = (A) 0.23, (B) 1.0, (C) 2.2, (D) 3.8, and (E) 6.3 g/min. Images (B)–(E) correspond to the same flow rates as those labeled (A)–(D) in Fig. 1.

air–polymer surface. In Fig. 6(C) the material near arrow 1 goes toward the surface region of the extrudate while the material at arrow 2 goes toward the core region. The extensional strain rate as the material flows from arrow 2 to the core region is much reduced from what occurs at the surface in Fig. 6(A). The surface region grows in size and eventually it peels off the sapphire [Fig. 6(D)], this is the surface failure. Once it peels off, the fracture line heals as the surface and core regions move off together.

We note that we observe a dark region that cyclically appears with the same frequency as sharkskin in the first 20 μm *upstream* of the exit. This coincides with the surface failure that occurs when the surface layer detaches from the exit region [Fig. 5(D)]. This dark ring could either be associated with a detachment from the inner surface of the capillary tube (adhesive failure), or could be caused by a breaking of the material right near the wall (cohesive failure). Due to the small length scales and weak optical contrast induced by this dark ring we do not seek to overinterpret this observation.

The visualization done here has qualitative similarities to that seen in the model materials referred to earlier in which the wavelengths and time scales are much greater [Inn *et al.* (1998)]. Thus much of the fundamental physics associated with the instability should carry over to the short wavelength and high frequency instability seen in polyethylenes. We see that the sharkskin instability is visible immediately after the tube exit. Previously, we observed no changes in the velocimetry within 20 μm upstream of the exit, while we see evidence of a crack in the last 20 μm. Thus we conclude that under the conditions of Fig. 1(B) that sharkskin is initiated in the region of $-20\,\mu\text{m} < x < 3\,\mu\text{m}$.

In Fig. 7, we show on-line micrographs for a series of mass flow rates. Note that the severity of the distortion increases with an increase in flow rate. These images can be compared to the postextrusion case where the extrudate cools down and crystallizes (Fig. 1). As the flow rate increases, the same two-layer structure is clearly visible; the difference is merely that the amplitude of distortion is larger.

The above experiments demonstrated sharkskin in the presence of stick or of weak slip. This result is typical for what was observed at temperatures of 177 °C and above. Here we reduce the temperature to 157 °C and find a different boundary condition. Figure 8 shows position versus time plots for particles near the wall at several flow rates. Strong sharkskin prevails in the three flow rates. The particles are inside the tube and the position $x = 0$ corresponds to the exit of the tube (similar to in Fig. 3). At a flow rate of 4.4 g/min, we observe a slight dip in the curve at $x = -75\,\mu$m. At higher flow rates, we see two or three kinks in the flow curve. By simultaneously observing the position of the particle inside the die and the sharkskin kinetics outside the die, we find that the period

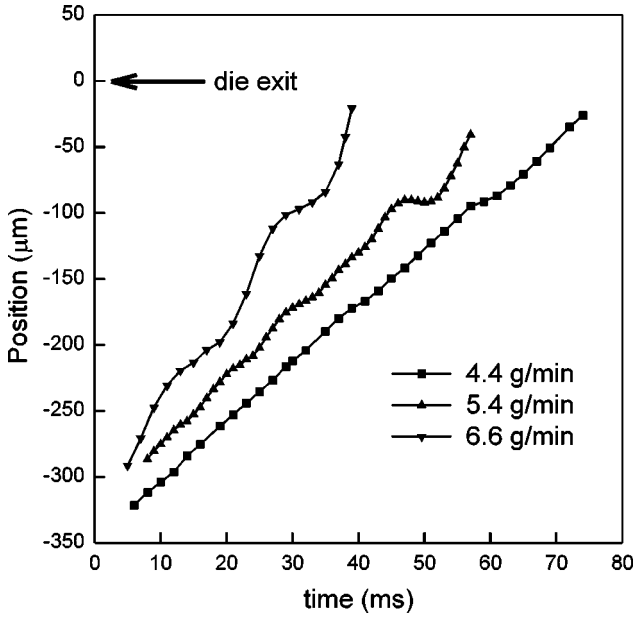

FIG. 8. Position–time curves for single particles as a function of the axial position in the vicinity of the die's exit. The three curves correspond to different flow rates. Oscillating stick–slip behavior is observed to have the same frequency as sharkskin. In this Figure $T = 157\,^{\circ}\mathrm{C}$ (whereas in all other figures the condition is $T = 177\,^{\circ}\mathrm{C}$).

between the kinks corresponds exactly to the period of sharkskin. Note that the severity of the kinks increases as the particle approaches the exit. We tentatively label this behavior as oscillating stick/slip. It is possible that this behavior is a result of the effects of oscillations in the stress due to the downstream sharkskin kinetics. Later we discuss why we believe that it is the sharkskin kinetics outside the tube that propagate a disturbance upstream and cause the stick/slip. For the remainder of the article, we return to the condition of $T = 177\,^{\circ}\mathrm{C}$.

BOUNDARY CONDITIONS, EXTENSIONAL DEFORMATION, AND SHARKSKIN

In order to assess the role of extensional flow at the exit as a potential cause of sharkskin, we measure the extensional strain rate in the bare surface and in the PPA treated surface. Our goal is two fold: to further quantify how the PPA eliminates sharkskin and to attempt to find the controlling parameter for the onset of it. As discussed in Sec. I, the upstream wall shear rate and total extensional deformation have previously been ruled out as possible controlling parameters for sharkskin. Since there is little change in the velocity profile from a position 2 mm upstream to 50 μm upstream, we also conclude that the shear rate near the exit is also not the controlling parameter for sharkskin. We focus on the polymer–sapphire surface upstream of the exit and on the polymer–air interface downstream of it, since this is where the largest extensional flows are anticipated. We combine velocimetry data at the wall upstream of the exit with that extracted from the sharkskin kinetics downstream of the exit. The results are shown in Fig. 9. Inside the die ($x < 0$) we conduct particle-tracking velocimetry of the particles that are nearest the wall. Outside the die, ($x > 0$) we conduct particle-tracking veloci-

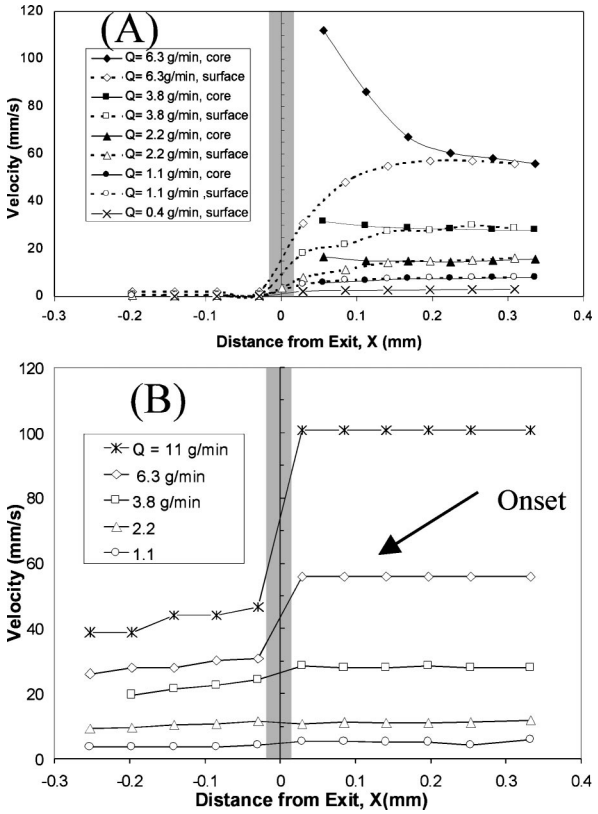

FIG. 9. Velocity of the polymer in the vicinity of the wall as it makes the transition from inside to outside the capillary die. For $x < 0$ (inside the die), the measurements were made of slow moving particles, i.e., those nearest the wall. For $x > 0$ (outside the die), the measurements were made at the air–polymer interface. The flow rate at which the onset of sharkskin is observed is noted. (A) Without the polymer process additive. For the higher flow rates, we show the velocity of both the core and the surface regions. (B) With the polymer process additive.

metry when there is no sharkskin present but we track the velocity of texture or structural elements in the case of sharkskin. Because it is difficult to simultaneously focus on the inner surface of the capillary and on the outer surface of the hot extrudate, we combine data from two sequential measurements, one taken inside the die and the other taken outside, thus we do not track the same material element from inside to outside. This region is shown in gray in the plots; the lines running through the gray are a guide to the eye.

For the case of polyethylene on sapphire [Fig. 9(A)], the measured velocity adjacent to the surface is near zero. Outside the tube, we track the velocity of both the surface and core regions in the immediate vicinity of the fracture line (labeled F in Fig. 5.) For the surface region (open circles), we track the velocity in the x direction (machine direction) at the fracture line. For the core region (closed circles), we track the velocity of the region closest to the leading edge of the same fracture surface. The general feature of the velocimetry is that, when the material first splits, the core is moving faster than the surface. In fact, for the higher throughputs, the core slows down as it moves further away from the capillary exit while the velocity of the surface region increases. Note the dramatic jump in velocity from inside the die to outside of the capillary tube at $x = 0$. The

actual distance over which this jump occurs has not been measured; the upper limit is the distance shown in the plot $\Delta x = 60\ \mu$m.

The detachment of the surface region, i.e. the secondary failure, is identifiable as the point at which the surface and core velocities become identical. For greater flow rates, the length (in the flow direction) is greater and, correspondingly, the point of detachment is further downstream (≈ 0.25 mm) whereas for a weaker flow rate this point is at ≈ 0.02 mm. For the weak flow rate of $Q = 1.0$ g/min, the sharkskin structure is too small to discern the point of detachment, so it is not possible to measure a difference between the velocities of the surface and of the core regions. The point of the onset of sharkskin is noted in this plot.

Upon addition of the polymer processing additive (PPA), there is a strong change in the flow profile of the LLDPE: the velocity does not go to zero at the wall as was seen in previously. In referring back to Fig. 2, we find substantial slippage at the LLDPE/PPA interface (closed squares). In Fig. 9(B), we show the surface velocimetry in the exit region when the surface has a fully developed coverage of PPA. The difference between this plot and that in the absence of PPA [Fig. 9(A)] is striking. First, the LLDPE is now slipping at its interface with the PPA; hence the velocity inside the capillary is well above zero. Second, the velocity inside the capillary is increasing as the exit is approached. Most important is the reduction in the velocity jump from inside to outside the capillary tube. This observation complements the stress birefringence measurements that show a reduction in stress at the exit when a low-energy surface is used [Piau *et al.* (1995)]. For the lower mass flow rates, the velocity is almost continuous across the exit. As the mass flow rate increases, there is a jump in velocity as the material traverses from inside to outside the die. The magnitude of the jump increases as the flow rate increases. This jump in velocity across the interface at high flow indicates that the PPA is not as effective in promoting slip at higher throughputs as it is at lower throughputs. This result was anticipated by Migler *et al.* (2001) when the extrapolation length b, defined as $b = \nu_s/\dot{\gamma}$, was found to be a decreasing function of throughput.

However, sharkskin is not completely eliminated by the addition of the PPA; it returns (albeit weakly) at a higher mass flow rate, as indicated in the plot. It is clear that the polymer is slipping at the interface from the behavior at $x < 0$. Earlier in this article we stated that sharkskin can occur under conditions of no slip, little slip, or oscillating stick/slip. Now we observe that sharkskin can also occur in the case of strong slip. Such a result is reasonable if the causative factor for sharkskin resides in the region just past the exit. As mentioned earlier, Wise *et al.* (2000) found sharkskin in a Teflon tube at sufficiently high flow rates. Since the polymer slips in the Teflon tube, their observation also indicates that sharkskin can occur under a slip boundary condition.

From the surface velocimetry data in the vicinity of the exit, it is obvious that the largest extensional strain rate occurs right at the exit. This is also the site of the initiation of sharkskin instability. In order to further interpret the data of Fig. 9, we consider the fluid flow in the region of the capillary exit. We define V_- to be the velocity of the slowest moving particles inside the capillary tube but as close to the exit as we can measure ($\approx 20\ \mu$m) and we define V_+ to be the velocity at the air–polymer interface $\approx 20\ \mu$m downstream from the exit. The extensional strain rate is defined as $\dot{\varepsilon} = d\nu/dx$ and at the exit the quantity we measure is

$$\dot{\varepsilon}_{\max} = \Delta V_{\text{exit}}/\Delta x, \tag{1}$$

where $\Delta V_{\text{exit}} = V_+ - V_-$ and Δx is the distance between these two points.

In Fig. 10 we present the results for $\dot{\varepsilon}_{\max}$. In the case of strong sharkskin, for the calculation of V_+ we utilized the velocimetry data of the surface layer, because this is

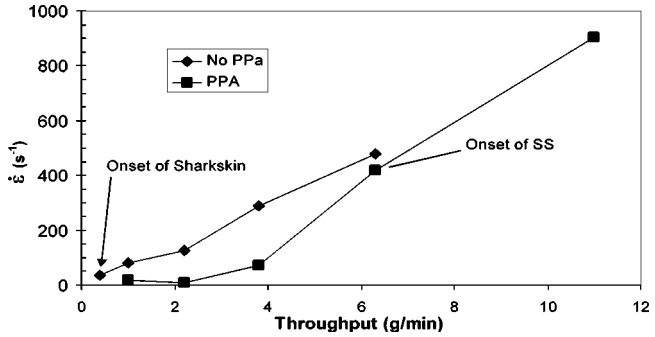

FIG. 10. Extensional strain rate at the polymer–air interface as the material exits the tube. We show cases with and without PPA. The onset of sharkskin is denoted by the arrows.

from the material that is continuous with the inner surface inside the capillary. However, beyond the onset of strong sharkskin, $\dot{\varepsilon}_{\max}$ should be considered as an apparent extensional strain rate, because the sharkskin makes the behavior too complex to quantify.

Cogswell suggested that the extensional strain rate may determine whether or not a material exhibits sharkskin. In Fig. 10 we show the maximum extensional strain at the onset of sharkskin for the cases with and without PPA. In the cases of PPA, $\dot{\varepsilon}_{\max} = 400\ \mathrm{s}^{-1}$ at the onset whereas in the case of no PPA, we have $\dot{\varepsilon}_{\max} \approx 80\ \mathrm{s}^{-1}$. The relative standard deviation in the *y* axis is 10%. The only change between these two cases is the boundary condition, yet $\dot{\varepsilon}_{\max}$ differs by a factor of approximately 5 between the two of them. Thus $\dot{\varepsilon}_{\max}$ is not the controlling parameter for the onset of sharkskin. While $\dot{\varepsilon}_{\max}$ at the onset of sharkskin is greater for the case with PPA than without, it was shown previously that the total extensional deformation is much *less* in the case of PPA than without [Migler *et al.* (2001)]. This leads us to consider that the parameter that describes the onset of sharkskin may be related to a product of the extensional strain rate and the total deformation.

In order to explore this possibility, we examine the flow rearrangements in the spirit of Cogswell (1977). In Poiseuille flow, at a distance $\delta R = R - r$ from the wall, the velocity profile is approximately linear when $\delta R \ll R$:

$$V_r = \frac{4V_f \delta R}{R}, \tag{2}$$

where we use the Newtonian approximation and neglect die swell. Here, R is the radius of the capillary, V_f is the final velocity of the extrudate, and r is the radial distance from the capillary axis. The corresponding wall shear rate is given by $\dot{\gamma}_w = 4V_f/R$. In the limit of $\delta R \ll R$, the maximum extensional strain rate (which occurs at the exit) has the same scaling: $\dot{\varepsilon}_{\max} \approx V_f/R$. Since $\dot{\gamma}_w$ and $\dot{\varepsilon}_{\max}$ have the same scaling, and since we have previously determined that $\dot{\gamma}_w$ is not the parameter that causes sharkskin, perhaps it should not be surprising that we found that $\dot{\varepsilon}_{\max}$ is also not the parameter that causes sharkskin.

To define the deformation rate, we consider a fluid element at the wall of width δR (in the radial direction). The total deformation of the material element from just inside the capillary tube to a point sufficiently outside the tube (so that there is only uniform translation of the extrudate) is

$$T = V_f/V_\delta. \tag{3}$$

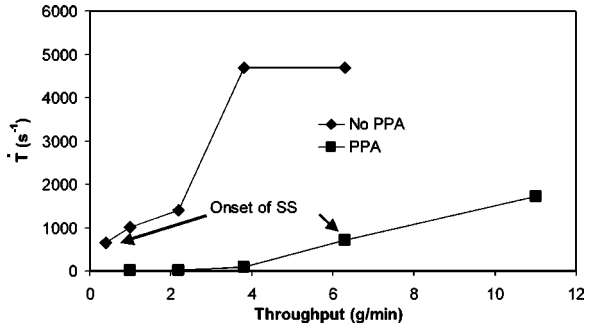

FIG. 11. Reconfiguration rate as a function of the flow rate for cases with and without PPA. The onset of sharkskin is denoted by the arrows.

Since we know that sharkskin initiates in the exit region, we use the measured value,

$$T = V_+ / V_- , \tag{4}$$

which is the deformation in the immediate vicinity of the exit. If we assume that the particle undergoes uniform acceleration as it goes from x_- to x_+, then the time it takes the particle to move between these two points is $\Delta t = 2\Delta x/(V_+ + V_-)$. We then define the *reconfiguration rate* by

$$\dot{T} = (T-1)/\Delta t. \tag{5}$$

We utilize $T-1$, rather than T, in the expression for $\dot{T}$, so that the reconfiguration rate would be zero in the case of a pure plug flow through the exit. Using Eqs. (1), (4), and (5), and the time for a particle to move by Δx, we have

$$\dot{T} = \dot{\varepsilon}_{\max}(T+1)/2. \tag{6}$$

In the case of a stick boundary condition, at the onset of sharkskin we are concerned with the case of $\delta R \ll R$ so that $T-1 \approx T$, and then $\dot{T} = \dot{\varepsilon}_{\max} T/2$ so that the reconfiguration rate is the product of the extensional strain rate and the extensional deformation.

In Fig. 11, we compare the values of $\dot{T}$ for the cases with and without PPA. Note that the addition of PPA causes a dramatic reduction in $\dot{T}$ for a given mass throughput. The relative standard deviation in the y axis is 10%. In referring back to Fig. 9(B), we see that the change in velocity across the exit is quite small for the lower throughputs, thus $\dot{T}$ (with PPA) is also quite small. As the jump in velocity across the exit increases in Fig. 9(B), so does the corresponding $\dot{T}$. Significantly, the onset of sharkskin as noted in this plot occurs for similar values of $\dot{T}$. This is the first measurable quantity that we have found which is comparable at the onset of sharkskin as the boundary condition is changed to from stick to slippage.

One could argue that the history of deformation, which is different with and without PPA, is the basis for an explanation for the onset of sharkskin in these two cases rather than what we propose. However Howells and Benbow (1962) observed that the deformation history does not strongly alter the onset of sharkskin (at least regarding the length of time in the die).

DISCUSSION

We can draw several conclusions regarding our work within the context of the literature on sharkskin. In terms of the stick or slip boundary conditions, perhaps it can now be understood why the results of some experiments have reported a stick boundary condition whereas others have reported a slip condition, and others have speculated about an oscillating stick/slip. We see here that *any of these boundary conditions is capable of producing sharkskin*. Of course the throughput at the onset is significantly affected by the flow boundary condition. While we can observe oscillating stick/slip, it is not the cause of sharkskin. The first reason is that sharkskin can be produced by other boundary conditions. Second, we find that the rough surface is caused by the tearing that occurs past the exit. Our observation of stick/slip localized to the exit is different from that of Mhetar and Archer (1998) who observed stick/slip in simple shear flow and from that of Munstedt *et al.* (2000) who observed global stick/slick in capillary flow.

Migler (2001) has shown previously that neither wall shear rate nor total extensional deformation is the parameter that controls the onset of sharkskin. Here we show that the extensional strain rate is also not the controlling parameter. In a viscoelastic liquid subjected to an imposed extensional rate of strain, extensional stress is a function of strain rate and time (or total deformation). Thus, to determine the stress to which the material is subjected, it is insufficient just to consider the strain rate—one must also consider the time scale (or total deformation). Thus we propose the simple product of extensional strain rate and extensional strain. The evidence presented here in favor of this idea is preliminary and must be backed up with more measurements. It is likely that $\dot{T}$ is only a first approximation to the actual parameter that causes sharkskin.

However, our conjecture is consistent with one of the earliest results in the sharkskin literature—that as one varies the radius of the capillary die, the onset of sharkskin occurs at the same value of the linear velocity of the extrudate [Howells and Benbow (1962)]. Here we make a simplified argument showing that $\dot{T}$ can explain this behavior. At the onset of sharkskin, we have shown that $\dot{T} \approx \dot{\varepsilon} T$. From the above considerations, we have

$$\dot{T} = \frac{V_f}{\delta R}. \tag{7}$$

The work presented in this article indicates that, beyond a critical value of $\dot{T}$, one finds the sharkskin instability. Since we consider δR to be the depth of the flow discontinuity at the onset of sharkskin, it is independent of the radius of the capillary tube. It is more dependent on our ability to measure the surface distortion in an on-line or quenched mode. Thus δR has the same value at different capillary radii. Equation (7) implies that $\dot{T}$ scales as the velocity of the extrudate. Thus, as the capillary radius varies, the onset of sharkskin occurs at the same critical value of $\dot{T}$, that is, when a critical extrudate velocity is reached. Alternatively, at the onset of sharkskin, the wall shear rate scales inversely with the capillary radius, independent of the length of the capillary.

This argument, combined with our data showing that the onset occurs for a comparable value of $\dot{T}$ for two very different boundary conditions, lends plausibility to the association of $\dot{T}$ with the onset of sharkskin. It is well known that it takes a finite time to build up a given level of extensional stress in a polymer. The stress is related to both the time of application of the deformation as well as the speed of deformation. Our results indicate that it is useful to compare slip and nonslip conditions at the onset of sharkskin. We find that, for the slip boundary condition, the total extensional deformation is signifi-

cantly less, but the rate of deformation is greater, leading presumably to the same level of stress so that the material fails cohesively at the polymer–wall–air interface. One anticipates that the critical value of $\dot{T}$ at the onset of sharkskin to be material dependent. Because $\dot{T}$ has the units of inverse time, it would be useful to compare our parameter with viscoelastic relaxation times.

CONCLUSION

We have examined the flow behavior of a linear low-density polyethylene in the immediate vicinity of the exit of a capillary die. We have shown that the three boundary conditions postulated in the literature can occur during sharkskin: stick, slip, and oscillating stick/slip. Thus the cause of sharkskin resides not in the flow boundary condition in the tube, but in the flow conditions just past the tube exit. The important parameter is the stretching rate just past the capillary exit. We have also shown that a two-layer model is correct for the sharkskin distortion in polyethylene, although we suggest that the ''reconfiguration rate,'' rather than the extensional strain rate determines the onset of sharkskin.

ACKNOWLEDGMENT

The authors wish to thank N. Cogswell for a critical review. Certain commercial equipment, instruments, or materials are identified in this article in order to adequately specify the experimental conditions. Such identification does not imply recommendation by the National Institute of Standards and Technology, nor does it imply that the materials are necessarily the best available for the purpose.

References

Amos, S. E., G. M. Giacoletto, J. H. Horns, C. Lavallée, and S. S. Woods, ''Polymer processing aids (PPA)'' in *Plastics Additives* (Munich, Hanser, 2001).

Barone, J. and S. Q. Wang, ''Flow birefringence study of sharkskin and stress relaxation in polybutadiene melts,'' Rheol. Acta **38**, 404–414 (1999).

Barone, J. R., N. Plucktaveesak, and S. Q. Wang, ''Interfacial molecular instability mechanism for sharkskin phenomenon in capillary extrusion of linear polyethylenes,'' J. Rheol. **42**, 813–832 (1998).

Barone, J. R., N. Plucktaveesak, and S. Q. Wang, ''Letter to the Editor: The mystery of the mechanism of sharkskin–Author's response,'' J. Rheol. **43**, 247–252 (1999).

Cogswell, F. N., ''Streching flow instabilities at the exits of extrusion dies,'' J. Non-Newtonian Fluid Mech. **2**, 37–47 (1977).

Denn, M. M., ''Extrusion instabilities and wall slip,'' Annu. Rev. Fluid Mech. **33**, 265–297 (2001).

Dhori, P. K., R. S. Jeyaseelan, A. J. Giacomin, and J. C. Slattery, ''Common line motion. 3. Implications in polymer extrusion,'' J. Non-Newtonian Fluid Mech. **71**, 231–243 (1997).

El Kissi, N. and J. M. Piau, ''Adhesion of linear low-density polyethylene for flow regimes with sharkskin,'' J. Rheol. **38**, 1447–1463 (1994).

El Kissi, N., L. Leger, J. M. Piau, and A. Mezghani, ''Effect of surface-properties on polymer melt slip and extrusion defects,'' J. Non-Newtonian Fluid Mech. **52**, 249–261 (1994).

El Kissi, N., J. M. Piau, and F. Toussaint, ''Sharkskin and cracking of polymer melt extrudates,'' J. Non-Newtonian Fluid Mech. **68**, 271–290 (1997).

Ghanta, V. G., B. L. Riise, and M. M. Denn, ''Disappearance of extrusion instabilities in brass capillary dies,'' J. Rheol. **43**, 435–442 (1999).

Hatzikiriakos, S. G. and J. M. Dealy, ''Wall slip of molten high-density polyethylenes. 2. Capillary rheometer studies,'' J. Rheol. **36**, 703–741 (1992).

Hatzikiriakos, S. G., P. Hong, W. Ho, and C. W. Stewart, ''The effect of Teflon (*Tm*) coatings in polyethylene capillary extrusion,'' J. Appl. Polym. Sci. **55**, 595–603 (1995).

Hong, Y., J. J. Cooper-White, M. E. Mackay, C. J. Hawker, E. Malmstrom, and N. Rehnberg, ''A novel processing aid for polymer extrusion: Rheology and processing of polyethylene and hyperbranched polymer blends,'' J. Rheol. **43**, 781–793 (1999).

Howells, E. R. and J. Benbow, ''Flow defects in polymer melts,'' Trans. Plastics Inst. **30**, 240–253 (1962).
Inn, Y. W., R. J. Fischer, and M. T. Shaw, ''Visual observation of development of sharkskin melt fracture in polybutadiene extrusion,'' Rheol. Acta **37**, 573–582 (1998).
Inn, Y. W., L. S. Wang, and M. T. Shaw, ''Efforts to find stick-slip flow in the land of a die under sharkskin melt fracture conditions: Polybutadiene,'' Macromol. Symp. **158**, 65–75 (2000).
Kalika, D. S. and M. M. Denn, ''Wall slip and extrudate distortion in linear low-density polyethylene,'' J. Rheol. **31**, 815–834 (1987).
Kulikov, O. L. and K. Hornung, ''A simple geometrical solution to the surface fracturing problem in extrusion processes,'' J. Non-Newtonian Fluid Mech. **98**, 107–115 (2001).
Mackley, M. R., R. P. G. Rutgers, and D. G. Gilbert, ''Surface instabilities during the extrusion of linear low density polyethylene,'' J. Non-Newtonian Fluid Mech. **76**, 281–297 (1998).
Mhetar, V. and L. A. Archer, ''Slip in entangled polymer melts. 1. General features,'' Macromolecules **31**, 8607–8616 (1998).
Migler, K. B., C. Lavallée, M. P. Dillon, S. S. Woods, and C. L. Gettinger, ''Visualizing the elimination of sharkskin through fluoropolymer additives: Coating and polymer–polymer slippage,'' J. Rheol. **45**, 565–581 (2001).
Moynihan, R. H., D. G. Baird, and R. Ramanathan, ''Additional observations on the surface melt fracture-behavior of linear low-density polyethylene,'' J. Non-Newtonian Fluid Mech. **36**, 255–263 (1990).
Munstedt, H., M. Schmidt, and E. Wassner, ''Stick and slip phenomena during extrusion of polyethylene melts as investigated by laser-Doppler velocimetry,'' J. Rheol. **44**, 413–428 (2000).
Person, T. J. and M. M. Denn, ''The effect of die materials and pressure-dependent slip on the extrusion of linear low-density polyethylene,'' J. Rheol. **41**, 249–265 (1997).
Piau, J. M., N. El Kissi, and A. Mezghani, ''Slip-flow of polybutadiene through fluorinated dies,'' J. Non-Newtonian Fluid Mech. **59**, 11–30 (1995).
Pomar, G., S. J. Muller, and M. M. Denn, ''Extrudate distortions in linear low-density polyethylene solutions and melt,'' J. Non-Newtonian Fluid Mech. **54**, 143–151 (1994).
Ramamurthy, A. V., ''Wall slip in viscous fluids and influence of materials of construction,'' J. Rheol. **30**, 337–357 (1986).
Rosenbaum, E. E., S. K. Randa, S. G. Hatzikiriakos, C. W. Stewart, D. L. Henry, and M. Buckmaster, ''Boron nitride as a processing aid for the extrusion of polyolefins and fluoropolymers,'' Polym. Eng. Sci. **40**, 179–190 (2000).
Rutgers, R. and M. Mackley, ''The correlation of experimental surface extrusion instabilities with numerically predicted exit surface stress concentrations and melt strength for linear low density polyethylene,'' J. Rheol. **44**, 1319–1334 (2000).
Tremblay, B., ''Sharkskin defects of polymer melts—The role of cohesion and adhesion,'' J. Rheol. **35**, 985–998 (1991).
Tzoganakis, C., B. C. Price, and S. G. Hatzikiriakos, ''Fractal analysis of the sharkskin phenomenon in polymer melt extrusion,'' J. Rheol. **37**, 355–366 (1993).
Venet, C. and B. Vergnes, ''Stress distribution around capillary die exit: An interpretation of the onset of sharkskin defect,'' J. Non-Newtonian Fluid Mech. **93**, 117–132 (2000).
Wang, S. Q., P. A. Drda, and Y. W. Inn, ''Exploring molecular origins of sharkskin, partial slip, and slope change in flow curves of linear low density polyethylene,'' J. Rheol. **40**, 875–898 (1996).
Wise, G. M., M. M. Denn, A. T. Bell, J. W. Mays, K. Hong, and H. Iatrou, ''Surface mobility and slip of polybutadiene melts in shear flow,'' J. Rheol. **44**, 549–567 (2000).
See EPAPS Document No. E-JORHD2-46-003202 for a video version of Fig. 5. This document may be retrieved via the EPAPS homepage (http://www.aip.org/pubservs/epaps.html) or from ftp.aip.org in the directory/epaps/. See the EPAPS homepage for more information.